JOURNAL OF GEOPHYSICAL RESEARCH, VOL. 94, NO. B6, PAGES 7250–7264, JUNE 10, 1989

Large Earthquakes and Crustal Deformation Near Taiwan

SILVIO K. PEZZOPANE[1] AND STEVEN G. WESNOUSKY

Center for Earthquake Research and Information, Memphis State University, Tennessee

Source parameters of 15 large ($m_b \geq 6$) earthquakes which occurred near Taiwan during the last 25 years are determined by synthetic seismogram analysis of teleseismic *P* and *S* waveforms. Source depths range from 13 to 88 km. Three earthquakes of intermediate depth are located within the southernmost limit of the Ryukyu arc and show thrust-type mechanisms with *T* axes subparallel to a northward dipping Wadati-Benioff zone. Shallow earthquakes (<30 km) are distributed over a broad region along and off the east coast of Taiwan and show both high-angle reverse and strike-slip mechanisms. The *P* axes of the shallow events located off the east coast of northern Taiwan are oriented near horizontal, trend south to southwest, and may reflect relative motion between the Okinawa platelet and Taiwan or complex deformation at the southwest limit of the Ryukyu Trench. In contrast, *P* axes of shallow earthquakes both onshore and off the east coast of central and southern Taiwan consistently trend northwest and are interpreted to reflect relative convergence between the Philippine Sea and Eurasian plates. Summation of the seismic moment tensors of eight large shallow earthquakes that occurred along and off the central and southern coast of Taiwan shows that relative plate motion between the Eurasian and Philippine Sea plates, when averaged over the last 25 years, has been accommodated by crustal contraction at a rate of 2.6–5.4 cm yr^{-1} along an azimuth of about 290°.

INTRODUCTION

Taiwan is located along the convergent boundary of the Eurasian and Philippine Sea plates (Figure 1). Plate convergence is accommodated to the northeast of Taiwan by northwestward subduction of the Philippine Sea plate beneath the Eurasian plate along the Ryukyu trench. In contrast, directly south of Taiwan, the Eurasian plate subducts southeastward beneath the Philippine Sea plate along the Manila Trench. Taiwan thus marks a segment of plate boundary where subduction undergoes a reversal in polarity. Furthermore, Taiwan marks the point where the Luzon island arc collided with the Eurasian continent as recently as 4 million years ago [e.g., *Angelier*, 1986; *Ho*, 1986]. To quantify better both the rate and the style of deformation currently taking place along this complex convergent plate boundary, we use synthetic seismogram techniques to determine the focal mechanism, source depth, source time history, and seismic moment of the 15 largest earthquakes that have occurred along the east coast and offshore of Taiwan during the last 25 years (Figure 2). The analysis provides the basis to determine the rate, style, and direction of relative plate motion that has been accommodated by large earthquakes near Taiwan during the last 25 years. Hence after a brief review of the regional plate tectonic framework and presentation of both the data and analysis, the results of the study are discussed in relation to current understanding of the relative motion between the Philippine Sea and Eurasian plates in the vicinity of Taiwan.

PLATE TECTONIC SETTING

A number of investigators have used earthquake slip vectors, transform fault trends, and marine magnetic anomalies to estimate the instantaneous pole of rotation vector between the Eurasian and Philippine Sea plates [e.g., *Fitch*, 1972; *Morgan*, 1972; *Seno*, 1977; *Chase*, 1978; *Minster and Jordan*, 1979]. Because of tectonic complexity, slip vectors from earthquakes adjacent to Taiwan have not been included in such determinations [e.g., *Seno*, 1977; *Minster and Jordan*, 1979]. The more recent of these studies [e.g., *Seno*, 1977; *Seno et al.*, 1987] predicts that the rate of relative convergence between the Philippine Sea and Eurasian plates is about 6.8 cm yr^{-1} in an azimuth 310° near Taiwan and provides a useful basis of comparison for our study (Figure 1).

Northeast of Taiwan, plate convergence is accommodated by subduction of the Philippine Sea plate beneath the Eurasian plate along the Ryukyu arc. Seismicity along the Ryukyu arc marks a well-defined Wadati-Benioff zone that dips north to northwest to a depth of over 230 km (Figures 2, 3*a*, and 3*b*). In contrast, seismicity across both northern and central Taiwan extends to depths no greater than about 120 km and does not form a distinct Wadati-Benioff zone (Figures 2 and 3*c*). The seismicity again extends to deeper depths as one moves south from Taiwan toward the Luzon Trough (Figures 1, 2, and 3*d*). Seismicity immediately south of Taiwan along the northern continuation of the Luzon arc forms an eastward dipping Wadati-Benioff zone that reaches to a depth of about 200 km (Figures 2 and 3*e*). Hence plate convergence along the east coast of central Taiwan may currently not be taken up by simple plate subduction but, rather, by extreme crustal shortening, as is evidenced in part by observations of strong folding [e.g., *Huchon et al.*, 1986; *Wu*, 1978], rapid uplift [e.g., *Jahn et al.*, 1986; *Taira*, 1975], and intense faulting [e.g., *Bonilla*, 1975; *Barrier and Angelier*, 1986] on the island of Taiwan.

Previous geologic and tectonic studies imply that the intense deformation on Taiwan reflects the active collision between the northern extension of the Luzon island arc, located on the western edge of the Philippine Sea plate, and the Chinese continental margin of the Eurasian plate [e.g., *Biq*, 1971; *Chai*, 1972; *Bowin et al.*, 1978; *Karig*, 1973; *Wu*, 1978]. The collision results in compression and uplift of Asiatic continental shelf sediments to form folded thrust sheets in central Taiwan and accretion of the Luzon volcanic arc to the coast of eastern

[1] Now at Department of Geology, University of Oregon, Eugene.

Paper number 89JB00351.
0148-0227/89/89JB-00351$05.00

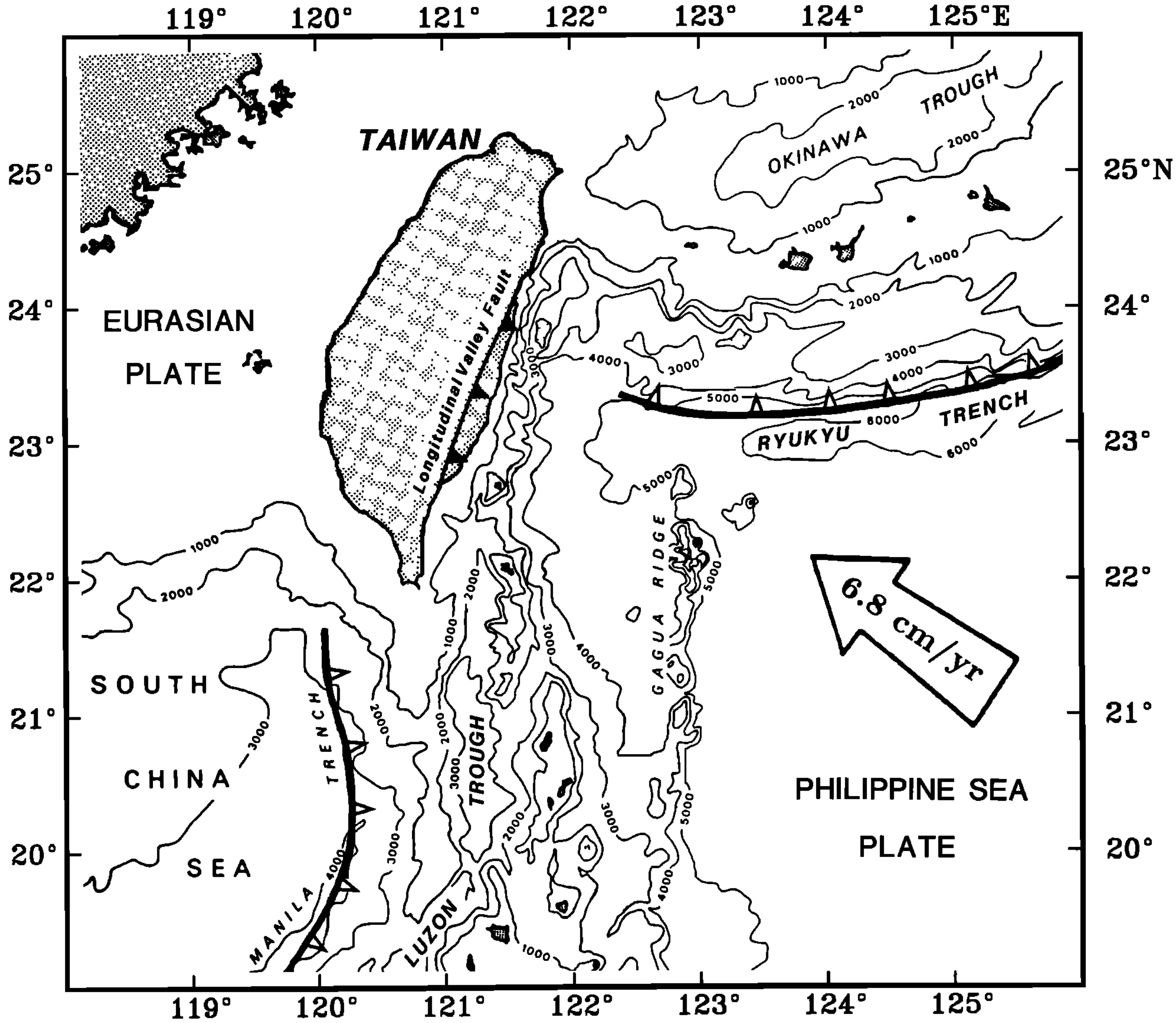

Fig. 1. Bathymetric and plate tectonic map of Taiwan and neighboring regions. Subduction along the Ryukyu and Manila trenches is represented by solid lines with large open barbs on the overriding plate. Arrow and number indicate the relative plate motion vector between the Philippine Sea and Eurasian plates determined by *Seno et al.* [1987]. Bathymetric contour intervals are 1000 m and from *Davis et al.* [1983]. The Longitudinal Valley fault strikes northward along the east coast of Taiwan and shows both reverse (closed barbs on the hanging wall) and left-lateral strike-slip movement [e.g., *Barrier*, 1985].

Taiwan [e.g., *Davis et al.*, 1983; *Suppe*, 1987]. Collision began about 4 million years ago and has propagated southward along the Luzon arc at a rate of about 90 km Ma^{-1} [e.g., *Barrier*, 1985; *Davis et al.*, 1983; *Suppe*, 1987]. The Longitudinal Valley fault (Figure 1) is an active reverse fault [e.g., *Allen*, 1962; *Hsu*, 1962; *York*, 1976] located along the east coast of Taiwan and is believed to represent the suture of the arc-continent collision [e.g., *Lee et al.*, 1978; *Barrier and Angelier*, 1986; *Pelletier and Stephan*, 1986].

Focal mechanism studies show that large earthquakes offshore and east of Taiwan are characterized by both strike-slip and reverse-type mechanisms [*Katsumata and Sykes*, 1969; *Sudo*, 1972*a*, *b*; *Seno and Kurita*, 1979; *Seno and Eguchi*, 1981; *Tsai*, 1986; *Wu*, 1970, 1978]. Partially, as a result, there exists a considerable diversity of opinion concerning the manner in which plate convergence near Taiwan is accommodated. For example, *Hsu* [1971], *Biq* [1971], and *Chai* [1972] interpret convergent plate motion near Taiwan to be taken up by east directed subduction. In contrast, *Jahn* [1972], *Juan* [1975], and *Juan et al.* [1980] suggest subduction in the opposite sense. *Fitch* [1972] concludes that a significant component of plate motion in Taiwan is taken up by left-lateral shear along the Longitudinal Valley fault, although recent studies suggest the fault is characterized by reverse faulting [e.g., *Barrier*, 1985]. Other investigators, in turn, argue that plate convergence along eastern Taiwan is taken up within a wide belt of shear deformation and not along a simple continuous plate boundary [e.g., *Hsu*, 1971; *Karig*, 1973; *Rowlett and Kelleher*, 1976; *Seno and Kurita*, 1979; *Wu*, 1978]. Thus a principal motivation for this study is to quantify the manner and rate at which relative motion along the plate boundary near Taiwan is accommodated.

Data and Analysis

Data used in this study are long-period *P* and *S* waveforms recorded on the World-Wide Standardized Seismograph Network (WWSSN) for the 15 largest ($m_b \geq 6$) earthquakes

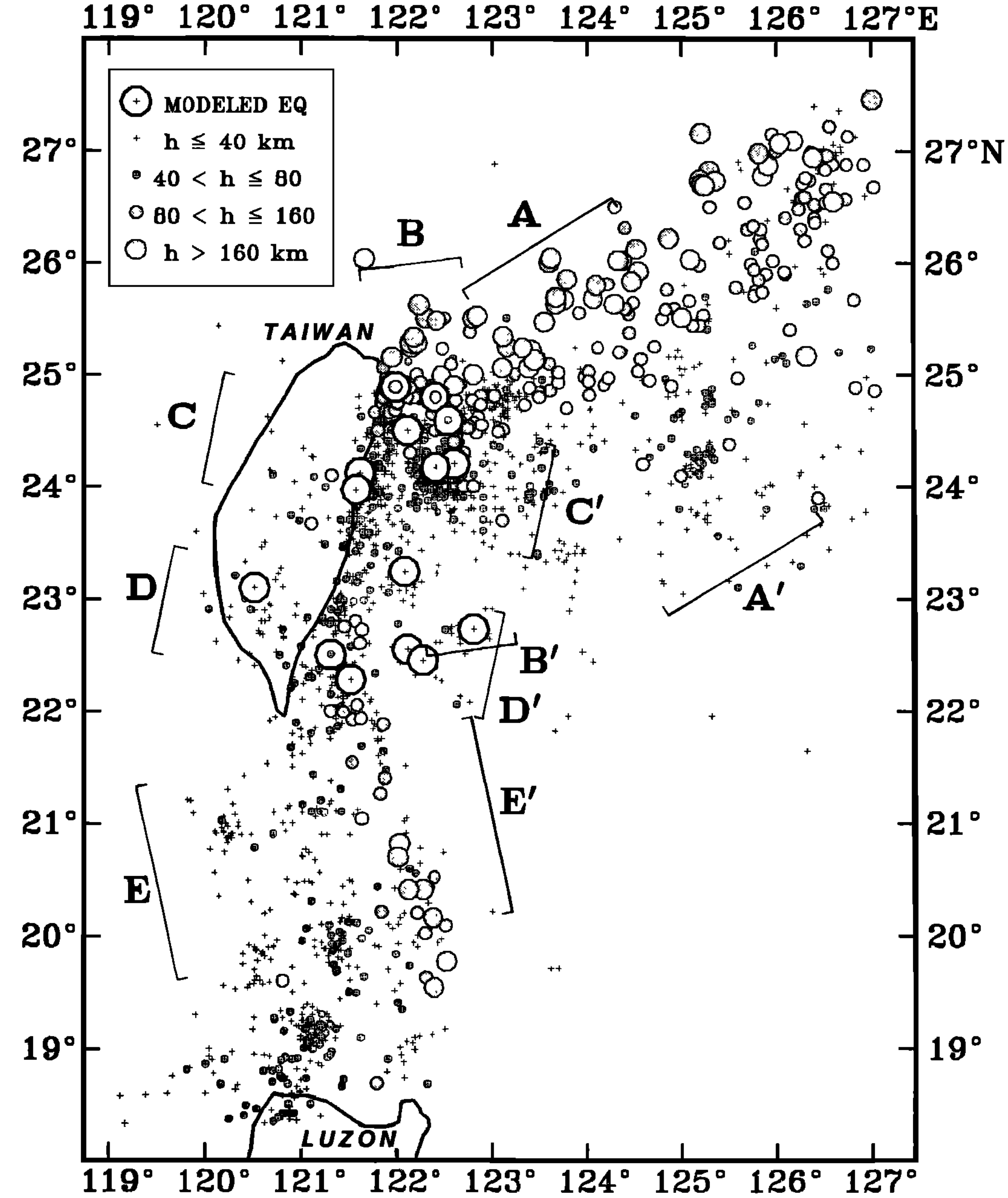

Fig. 2. Epicenters of $m_b \geq 3$ earthquakes near Taiwan taken from the Preliminary Determination of Epicenters (PDE) catalog for the period 1960 to July 1986. Symbol size and type are plotted as a function of h, the hypocentral depth. Large open circles show the location of the earthquakes examined in this study. Large letters and brackets denote the orientation and extent of seismicity plotted on the vertical cross sections shown in Figures 3*a*–3*e*.

listed in the Preliminary Determination of Epicenters (PDE) catalog that occurred between 1963 and 1988. Epicentral data for each event are listed in Table 1.

P wave first motions are used to determine an initial focal mechanism for each event. Synthetic P and SH waveforms are computed for each earthquake using the techniques of *Langston and Helmberger* [1975]. The primary factors controlling the shape of the synthetic waveforms are the focal mechanism, focal depth, source time function, attenuation, and velocity-density structure. A forward modeling approach is used to match the synthetic to the observed WWSSN waveforms to define better the focal mechanism and to determine the focal depth, source time history, and seismic moment for each event. Complications due to upper mantle and core structures are avoided by considering only waveforms recorded at epicentral distances of 30° to about 90°. Takeoff angles are calculated assuming a P velocity of 7.75 km s^{-1} and S velocity of 4.35 km s^{-1} in the vicinity of the earthquake source. The density ρ at the source is assumed to be 3.2 g cm^{-1}. Focal depth and reflection coefficients for surface bounces of the depth phases (pP, sP, and sS) are calculated using an assumed average P and S velocity above the source of 6.4 km s^{-1} and 3.7 km s^{-1}, respectively, and ρ at the surface is assumed to be 2.6 g cm^{-1}. The velocity and density values used here are consistent with the estimates of *Roecker et al.* [1987] and *Wu* [1978]. Attenuation of the seismic waves is taken into account using *Futterman's* [1962] attenuation operator, assuming values of t^* equal to 1.0 and 4.0 s for P and S waves, respectively.

The source parameters determined from the waveform analysis for each event are summarized in Table 2 and Figure

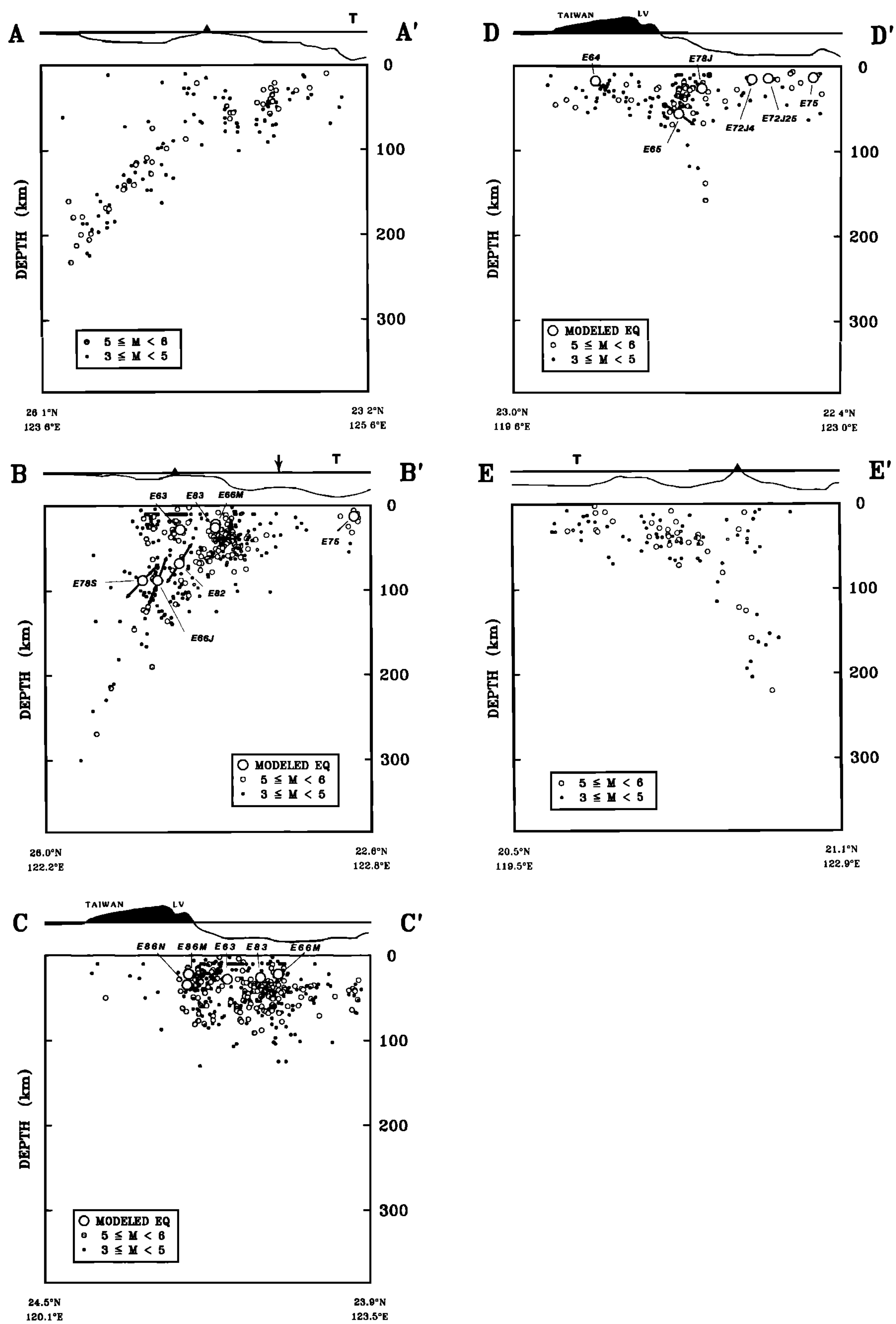

Fig. 3. Hypocenters of $m_b \geq 3$ earthquakes in the period 1960–1986 listed by PDE are projected onto vertical cross sections, with orientation as shown in Figure 2. Cross sections are true scale, taken perpendicular to the apparent structural trends. Large circles denote the $m_b \geq 6$ earthquakes in this study. Bathymetry is shown above each section, with vertical exaggeration of about 5. *T* indicates the trench axis. Triangles denote the volcanic chain. Diverging arrows near large circles denote orientation of relative tension axis (*T* axis) for intermediate-depth focal mechanisms determined in this study. Large arrow on upper section in Figure 3*b* indicates the east-west boundary at 23.5°N latitude, north of which the Philippine Sea plate begins to subduct beneath the Ryukyu arc [e.g., *Hagen et al.*, 1988]. On the upper section Figures 3*c* and 3*d* the solid area marks Taiwan and LV denotes the Longitudinal Valley fault.

TABLE 1. Epicentral Data

Event	Date	Origin Time	Latitude, °N	Longitude, °E	m_b
E63	Feb. 13, 1963	0850:04.5	24.50	122.10	6.2
E64	Jan. 18, 1964	1204:40.0	23.10	120.50	5.9
E65	May 17, 1965	1719:25.9	22.50	121.30	6.2
E66M	March 12, 1966	1631:20.6	24.20	122.60	6.6
E66J	July 1, 1966	0550:38.8	24.80	122.40	6.2
E72J4	Jan. 4, 1972	0316:54.5	22.55	122.10	6.1
E72J25	Jan. 25, 1972	0206:23.3	22.45	122.26	6.3
E75	March 23, 1975	0732:36.5	22.73	122.80	6.2
E78J	July 23, 1978	1442:36.9	22.28	121.51	6.5
E78S	Sept. 2, 1978	0157:33.4	24.89	121.98	6.1
E78D	Dec. 23, 1978	1123:12.0	23.24	122.07	6.6
E82	Dec. 17, 1982	0243:03.6	24.59	122.54	6.1
E83	June 24, 1983	0906:45.8	24.17	122.40	6.1
E86M	May 20, 1986	0525:46.9	24.12	121.61	6.1
E86N	Nov. 14, 1986	2120:10.5	23.97	121.57	6.3

Data are from preliminary determination of epicenters (PDE) earthquake catalog. (National Earthquake Information Center, National Geophysical Data Center, Boulder, Colorado).

4. Figures showing the observed versus synthetic waveforms, the P wave first motions, and the source parameters determined for each event are placed separately in the appendix. For reference, aftershocks listed by PDE which occurred within 48 hours after each respective mainshock are plotted in Figure 5.

Discussion

Intermediate-Depth Earthquakes

Four of the 15 large earthquakes examined occurred at intermediate depths ranging from 56 to 88 km. Three (E66J, E78S, E82) of the four events at intermediate depth are located at the northern end of the study area and show source depths ranging from 68 to 88 km (Figure 4). The three events appear to locate within the downgoing Philippine Sea plate and show thrust-type mechanisms with T axes oriented in the downdip direction of the inclined Wadati-Benioff zone (Figures 3*b* and 4). Such a T axis orientation has been observed for intermediate and deep focus earthquakes located within many of the Wadati-Benioff zones around the world and has generally been attributed to gravitational forces acting on the sinking slab [e.g., *Isacks and Molnar*, 1969; *Ruff and Kanamori*, 1983; *Astiz*, 1987]. The northerly striking and steeply dipping nodal planes associated with two (E78S and E82) of the three northern events may reflect hinge-faulting within the subducting slab [*Astiz*, 1987]. Downdip gravitational forces may also explain the mechanism of the intermediate-depth event E65 which occurred in the southern portion of the study area and shows a T axis subparallel to a poorly defined east dipping Wadati-Benioff zone (Figures 3*d* and 4).

Shallow Earthquakes

The 11 shallow earthquakes studied range in depth from 13 to 28 km, show both strike-slip and high-angle reverse-type focal mechanisms, and are distributed over a broad area (Figure 4). The pattern of epicenters and mechanisms does not appear to reflect convergent plate motion along a shallow interplate thrust plane, as is interpreted along most of the circum-Pacific convergent plate boundaries. Rather, the distribution of epicenters and the mix of focal mechanisms

TABLE 2. Body wave Mechanisms and Source Parameters

Event	Depth h, km	Strike ϕ, °	Dip δ, °	Rake λ, °	Rise Time τ, s	Rupture Duration τ_c, s	Seismic Moment M_0*	Number of Stations for M_0
E63	28	16	58	150	2.6	5.2	10.0 ± 1.4	11
E64	18	15	50	100	1.5	3.0	0.4 ± 0.1	14
E65	56	188	60	20	4.0	4.5	2.7 ± 0.4	21
E66M	22	130	76	18	1.5	5.5	48.6 ± 9.6	3
E66J	88	126	64	80	1.0	2.0	0.7 ± 0.1	26
E72J4	15	158	56	33	2.0	4.0	1.1 ± 0.8	15
E72J25	14	336	86	10	2.0	4.0	13.4 ± 2.8	8
E75	13	328	84	3	2.0	5.0	2.8 ± 0.9	13
E78J	26	355	42	62	1.0	4.5	4.6 ± 1.3	14
E78S	88	164	70	46	1.0	3.0	0.8 ± 0.1	19
E78D	18	200	40	90	1.0	3.5	1.9 ± 0.3	25
E82	68	164	64	56	1.5	4.0	0.6 ± 0.1	16
E83	24	88	72	90	3.5	6.0	0.7 ± 0.1	25
E86M	22	45	50	90	0.8	2.4	0.5 ± 0.1	15
E86N†	14	43	57	100	—	—	17.0	—

*Units of 10^{26} dyn cm; 95% confidence limits computed with assumption of Student's t distribution.
†Source parameters determined by *Hwang and Kanamori* [1989].

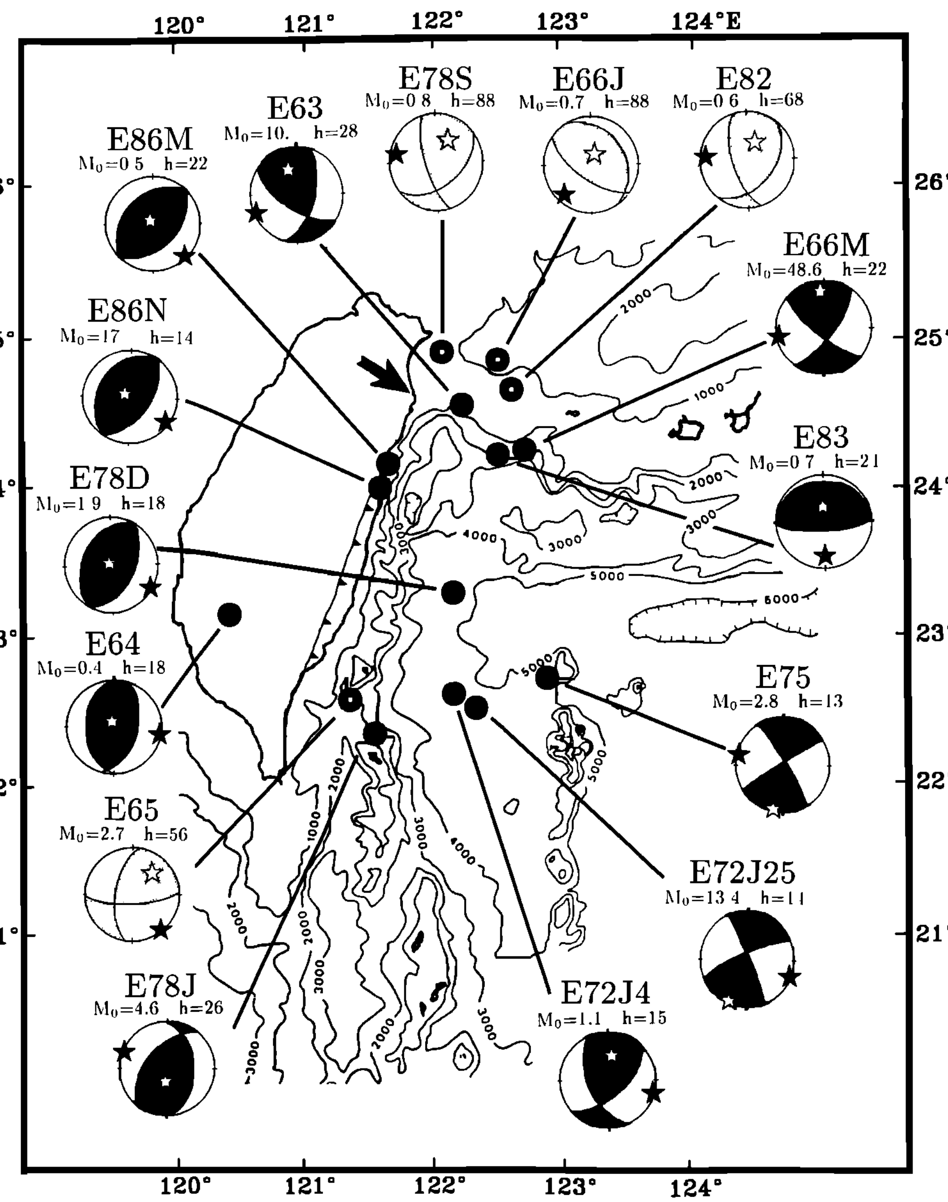

Fig. 4. Focal mechanism solutions and source parameters determined from the waveform analysis. Event labels (e.g., E64) correspond to Table 2. Mechanisms are lower hemisphere equal-area projections with compressional first motion quadrants either shaded or solid for intermediate or shallow depth earthquakes, respectively. Open star is T axis and solid star is P axis. Listed above each mechanism is the seismic moment and source depth in units of 10^{26} dyne cm and kilometers, respectively. The source parameters of E86N are from *Hwang and Kanamori* [1989]. Bathymetric contour intervals [*Davis et al.*, 1983] are 1000 m, and the arrow shows the trend of a prominent bathymetric escarpment discussed in the text.

observed suggests that, at least in part, relative plate motion is being taken up by distributed deformation of the Earth's crust. *Kostrov* [1974] showed that the average rate of strain $\dot{\varepsilon}_{ij}$, in a region where earthquakes are distributed uniformly throughout a seismogenic volume V, is proportional to the sum of the seismic moment tensors $\Sigma\, M_{ij}$ of all earthquakes occurring in the volume per unit time T;

$$\dot{\varepsilon}_{ij}=\frac{1}{2\mu VT}\left(\sum_{x=1}^{N} M_{ij}^{(x)}\right) \tag{1}$$

The seismic moment tensor M_{ij} is a direct measure of the deformation resulting from the occurrence of an earthquake and is completely described when the strike, dip, and rake are known in addition to the scalar value of the seismic moment M_0 [e.g., *Aki and Richards*, 1980]. The P, T, and B axes of focal mechanism solutions correspond to the principal axes of the moment tensor. We can use (1) and the source parameters determined for the large, shallow earthquakes to estimate both the rate and direction of crustal shortening accommodated by large earthquakes during the last 25 years in Taiwan. Although we consider only the largest earthquakes that have occurred during the last 25 years, it has been shown that events of smaller size contribute only a small fraction to the total seismic moment release and hence crustal deformation in tectonic areas [*Brune*, 1968].

The historical record of large, shallow earthquakes near Taiwan is plotted as a map of epicenters in Figure 6. Large

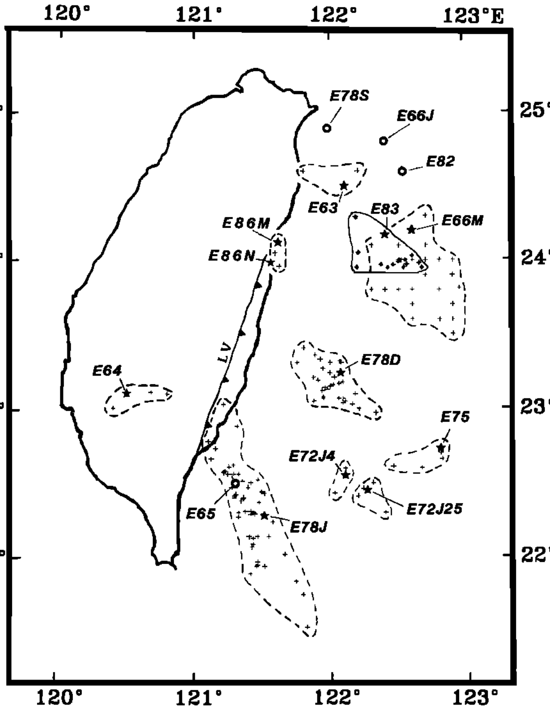

Fig. 5. Map of all aftershocks recorded by PDE which occurred 48 hours after the main shock. Open circles denote intermediate-depth main shocks with no reported aftershocks. Stars indicate mainshocks with aftershocks shown as pluses. LV indicates the Longitudinal Valley fault.

earthquakes during the last 25 years are distributed within a zone of seismicity that extends 400 km by 280 km in the north and east directions, respectively (dotted box, Figure 6), and are limited to depths of less than 30 km. On that basis we initially define a seismogenic volume characterized by dimensions of 400, 280, and 30 km, respectively. Additionally, we have determined the strike, dip, rake, and scalar value of the seismic moment (M_0) and hence uniquely define the seismic moment tensor $\bar{M}$ of each of the events in this study [e.g., *Aki and Richards*, 1980]. Summing the moment tensors ($\Sigma \bar{M}$) of each of the 11 shallow events and using (1) (assuming $\mu = 3 \times 10^{11}$ dyn cm^{-2}), we find the rate of horizontal compressive strain across the volume, averaged over the last 25 years, is maximum at an azimuth 272° and equals 1.6×10^{-7}yr^{-1}. Multiplying the maximum horizontal strain rate by the distance across the deforming volume (270 km) indicates easterly contraction of the crust has averaged about 4.4 cm yr^{-1} during the last 25 years. For comparison, the rate (4.4 cm yr^{-1}) and direction (272°) of maximum crustal shortening determined here is about 65% of the long-term plate convergence rate (6.8 cm yr^{-1}) and rotated about 40° counterclockwise from that predicted by *Seno et al.* [1987], respectively. The result is summarized in Figure 7*a*. Further, assuming only a 275 km north-south dimension for the seismogenic volume, which is sufficient to encompass only the last 25 years of large earthquakes, would result in a 50% increase in the rates just calculated. However, such an estimate would not account for the spatial averaging of seismic moment release which likely occurs over longer periods of time, as evidenced by the distribution of historical seismicity in Figure 6.

The apparent discrepancy between the direction of relative plate motion predicted by plate models and that computed here is probably due to considering an area which encompasses more than one stress regime. More specifically, the summary of focal mechanisms (Figure 4) shows that the three northernmost shallow events (E63, E66M, and E83) are located north of the presumed westward extension of the Ryukyu trench (Figure 1) [*Hagen et al.*, 1988; *Bowin et al.*, 1978] and show *P* axes oriented near horizontal and trending south to southwest. In contrast to those three shallow northern events, the remaining eight shallow earthquakes located onshore and off the east coast of central and southern Taiwan consistently show *P* axes which trend northwest. Thus to quantify more accurately the details of crustal deformation, the northern and southern regions should be considered separately. Initially then, we consider the three northernmost events and follow that by analysis of the remaining events to the south.

A seismogenic volume characterized by a thickness of 30 km and areal dimensions of 125 km × 125 km is of sufficient size to encompass the three shallow earthquakes to the north (Figure 7*b*). Substituting these volumetric dimensions and the seismic moment tensors for events E63, E66M, and E83 (Table 2) into (1) yields estimates of the direction and rate of maximum horizontal contraction of the crust. In this case the direction of maximum contraction of the crust is found at an azimuth of 261°, and the rate of horizontal compressive strain and crustal shortening are 7.5×10^{-5}yr^{-1} and 9.3 cm yr^{-1}, respectively (Figure 7*b*). The rates of strain and shortening determined for this case are not significant since the calculation is based on only three earthquakes which occurred in a short period of time and which are not sufficient to define well a seismogenic volume. Furthermore, the calculation includes the largest event (E66M, $M_0 = 48.6 \times 10^{26}$ dyn cm) in the data set. The

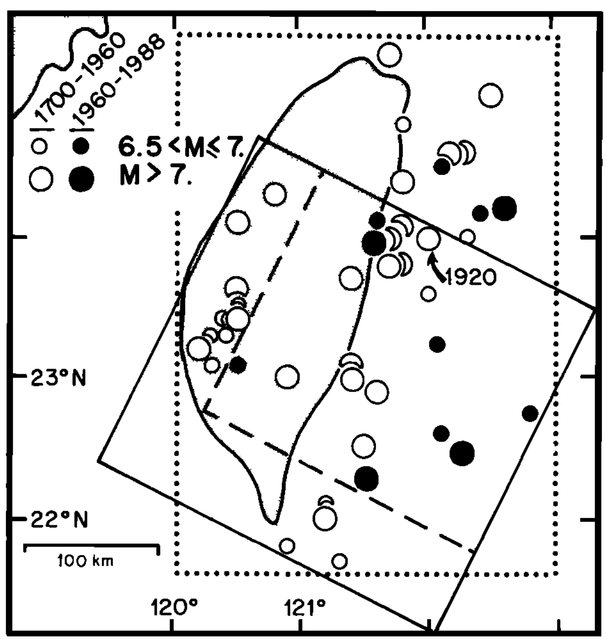

Fig. 6. Epicenters of shallow earthquakes of $M \geq 6.5$ near Taiwan during the period from 1788 to 1960 are shown by open symbols. Epicenters of large events that occurred after 1960 (Table 2) are shown by closed symbols. Solid and dashed boxes represent areal dimensions of seismogenic volumes used to compute crustal deformation rates in this paper. Data for the periods before 1900, 1900–1960, and 1960 to present are from *Tsai* [1985], *Hsu* [1971], and this paper, respectively. Magnitudes of earthquakes after 1960 are computed from moments determined in this paper using the empirical relationship $\log M_0 = 1.5M + 16.1$ [*Kanamori*, 1973].

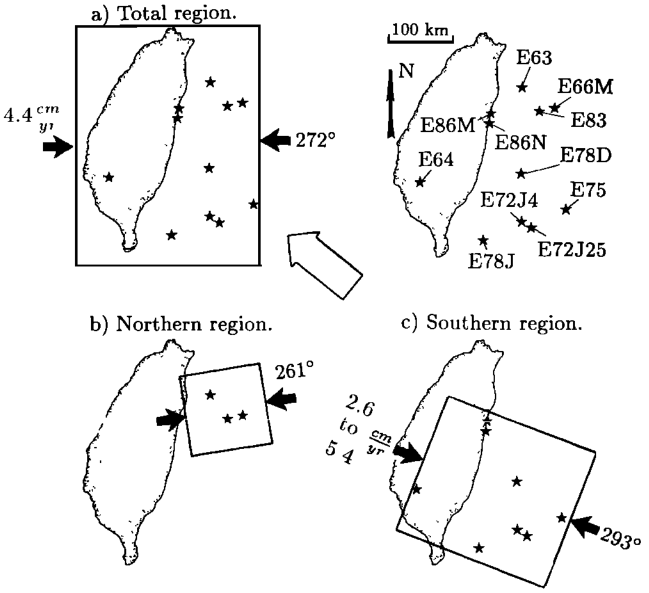

Fig. 7. Regional averages of the orientation and rate of maximum horizontal crustal shortening for (*a*) the total region, (*b*) the northern region, and (*c*) the southern region of Taiwan, calculated from the past 25 years of seismicity. Boxes represent the areal dimensions of 30-km-thick seismogenic volumes enclosing the shallow earthquakes (stars) used to calculate crustal shortening. Estimates of the rate and azimuth of maximum horizontal crustal shortening is indicated to the left and right of each box, respectively. Large open arrow indicates the direction of relative plate convergence determined by *Seno et al.* [1987]. See text for complete discussion.

direction of maximum crustal contraction, however, is not affected by the choice of seismogenic volume and indicates that the direction of maximum contraction determined here (261°) is rotated about 50° counterclockwise as compared to the direction of relative plate motion (310°) predicted by regional plate tectonic models (Figure 7) [e.g., *Seno et al.*, 1987; *Minster and Jordan*, 1979].

The difference between the observed direction of crustal shortening in the northern region (Figure 7*b*) and the predicted direction of plate convergence implies that the northernmost shallow events do not solely reflect the relative motion between the Philippine Sea and Eurasian plates. For example, *Sibuet et al.* [1987] suggest the occurrence of an Okinawa platelet based on en échelon extensional grabens in the Okinawa Trough (Figure 8). *Sibuet et al.* [1987] note that the left-stepping orientation of the en echelon extensional grabens are consistent with right-lateral shear and a southwestward component of strike-slip movement of the Okinawa platelet with respect to Eurasia. If indeed this is the case, impingement of the southwest end of the Okinawa platelet into Taiwan would produce southwest trending compression offshore northern Taiwan, consistent with the direction of maximum crustal shortening offshore northern Taiwan (Figure 7*b*). It is also possible that more local effects are responsible for rotation of the *P* axis orientations of earthquakes in the northern region. For example, the shallow events (E63, E66M, and E83) in the northern region and three $m_b > 5.8$ earthquakes shown by *Wu* [1978] locate along the edge of a prominent northwest trending bathymetric escarpment (arrow, Figure 4). The focal mechanisms of the earthquakes near the escarpment have in common a northwest striking nodal plane that trends parallel to the escarpment. The seismicity in the region near the bathymetric shelf is possibly related to the termination of intermediate-depth seismicity associated with Philippine Sea plate subduction (Figure 2). Perhaps earthquakes that locate along the bathymetric shelf reflect complex deformation at the junction where the lateral edge of the subducting Philippine Sea plate collides with the crust of Taiwan.

The eight remaining shallow earthquakes are spread over a region to the south that defines a seismogenic volume of 30 km thickness and has areal dimensions of 225 km × 200 km in the northwest and northeast directions, respectively (dashed box, Figure 6). However, the historical record of earthquakes suggests that the recent earthquakes studied here define but a portion of a wider seismogenic volume characterized by northwest and northeast areal dimensions of 280 km × 260 km, respectively (solid box, Figure 6). The volumes are placed approximately orthogonal to the relative plate motion vector of *Seno et al.* (1987), and the range of dimensions place reasonable bounds on the volume of the crust, which is currently accommodating seismic deformation in the vicinity of central and southern Taiwan. Summation of the seismic moment tensors and use of these two volumes yields estimates of the maximum horizontal compressive strain and shortening of the crust which range from $1.2–1.9 \times 10^{-7} yr^{-1}$ and 3.4–4.3 cm yr^{-1}, respectively, at an azimuth 293°. The direction of maximum contraction is in general accord with the relative plate motion (310°) predicted by the instantaneous poles of rotation between the Eurasian

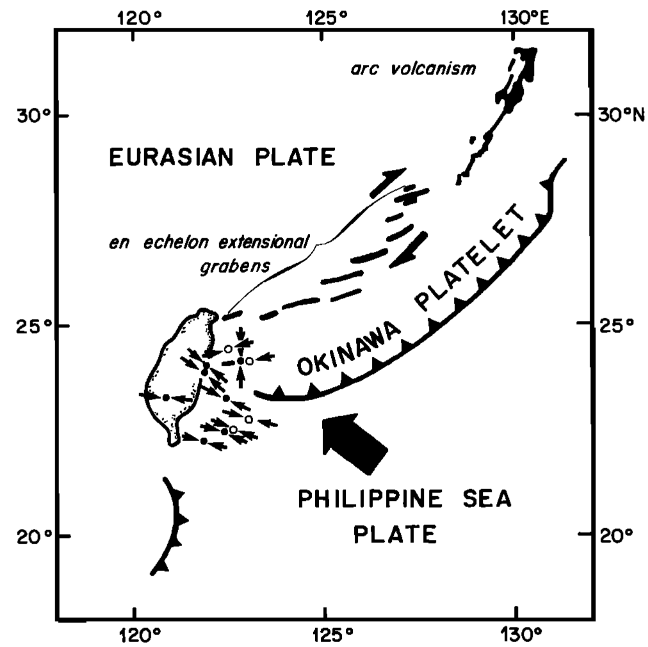

Fig. 8. Simplified diagram of the kinematics of the Okinawa platelet modified from *Sibuet et al.* [1987]. The Okinawa platelet, according to Sibuet et al., is bounded to the northwest by en echelon extensional grabens and back arc volcanism (thick lines) in the Okinawa Trough and to the southwest by Ryukyu Trench (lines east of Taiwan with open barbs on the overriding plate). Large half-sided arrows denote inferred relative right-lateral motion of the Okinawa platelet with respect to the Eurasian plate. Open and closed circles with arrows indicate the trend of the *P* axes of strike-slip and reverse-type earthquakes, respectively. Large solid arrow shows the computed average direction of crustal shortening (293°) for the southern region (Figure 6*c*). The southwest end of the Okinawa platelet may converge with Taiwan to generate maximum crustal shortening along a southwest direction offshore northern Taiwan.

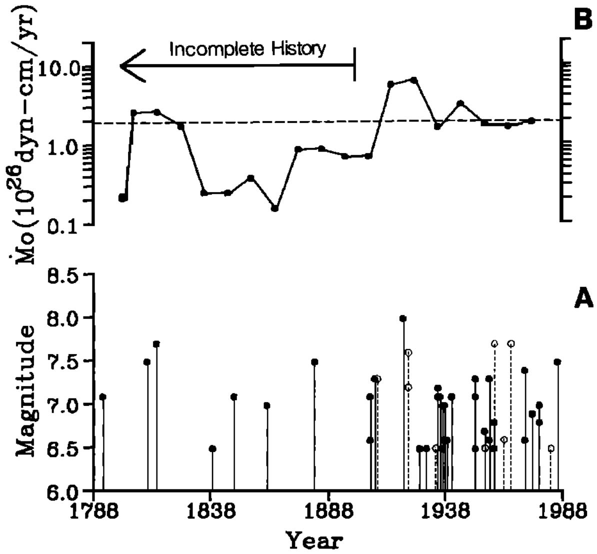

Fig. 9. (*a*) Large, shallow earthquakes near Taiwan plotted as a function of magnitude versus time. Events plotted within and outside the solid box in Figure 6 are shown here as solid and open symbols, respectively. (*b*) Plot of the 25-year running average (dots) of the seismic moment release rate for shallow earthquakes located within the solid box shown in Figure 6. Data points in the running average are placed in the middle of the time period sampled. The horizontal dashed line is the average rate of seismic moment release calculated from the entire 200-year record.

and Philippine Sea plates (Figure 6) [*Seno et al.*, 1987; *Minster and Jordan*, 1979]. Hence deformation of the crust resulting from earthquakes in the southern region is interpreted to reflect primarily the relative motion between the Eurasian and Philippine Sea plates. However, the rate of crustal shortening (3.4–4.3 cm yr^{-1}) is much less than the rate of plate convergence (6.8 cm yr^{-1}) predicted by plate tectonic models. The difference in the values of the rates may be interpreted to indicate that a portion of relative plate motion is accommodated by aseismic processes or that estimates of plate convergence based on seafloor magnetic anomalies do not accurately reflect current rates of relative plate motion. With regard to these latter hypotheses, it is important to consider in some detail the uncertainties associated with the deformation analysis presented here.

The WWSSN station distribution for events in the vicinity of southern Taiwan is generally excellent (see the appendix), and as a result, focal mechanisms are generally well defined. Similarly, estimates of the scalar values of M_0 for earthquakes in the southern region are generally based on observations at 10 or more stations for each event (Table 2). Taking the extremum of the 95% confidence limits associated with the mean value of seismic moment estimated for each event (Table 2), which provides a measure of uncertainty to the estimates of M_0, would yield only about a 25% change in the moment sum calculated from the eight shallow earthquakes in the southern region. The uncertainty translates linearly into the estimate of crustal shortening. Hence a more realistic limit on the rate of crustal shortening in the southern regions is 2.6–5.4 cm yr^{-1}. It seems unlikely that errors in the determination of seismic moment tensors could account for the difference between the rate of convergence predicted by plate tectonic models (6.8 cm yr^{-1}) and the rate (2.6–5.4 cm yr^{-1}) of crustal shortening computed here. However, in addition to the uncertainties attendant to the computation of seismic moments there exists further uncertainty in the estimates of crustal shortening rates, which arises from the short period of time we have considered.

The historical record of seismicity of Taiwan extends back more than 200 years but is considered complete only back to about 1900 [*Hsu*, 1971]. The map of epicenters in Figure 6 shows that the most recent 25 years of seismicity does not fully reflect the spatial distribution of earthquakes characteristic of the Taiwan region. In that regard the uncertainty associated with defining the seismogenic volume for computing crustal shortening rates with equation (1) has been taken into account by making the calculations for the maximum and minimum reasonable volumes which encompass the earthquakes in the southern region (dashed and solid boxes, Figure 6). However, such does not take into account the question of whether or not the rate of seismic moment release averaged over 25 years is representative of longer-term rates of deformation.

The historical record of Taiwan earthquakes of shallow depth is further shown as a plot of magnitude versus time in Figure 9*a*. Magnitudes for events after 1960 are converted from the estimates of seismic moment listed in Table 2 using the relationship Log M_0 = 1.5M + 16.1 [*Kanamori*, 1983]. Data for earthquakes before 1900 and from 1900 to 1960 are from *Tsai* [1985] and *Hsu* [1971], respectively. The magnitudes in each catalog are scaled to the magnitudes of *Gutenberg and Richter* [1954] and hence are generally equivalent to surface wave magnitude M_s and may also be converted to estimates of seismic moments using the preceding relationship between M and M_0. Figure 9*b* shows the 25-year running average of seismic moment release of earthquakes in the southern region (solid box, Figure 6). Seismic moment release during the most recent 25-year period of time is less than observed during similar periods of time in the first half of this century and generally higher than values estimated for the period prior to 1900. The higher rates during the first half of this century are dominated by the occurrence of the great M=8.0 [*Abe*, 1981] earthquake of 1920 (Figure 6). The lesser values of seismic moment rate observed prior to 1900 are likely due to an incomplete historical record. The rate of seismic moment release averaged over the last 200 years (dashed line, Figure 9*b*) is virtually equal to the rate calculated for the last 25 years. With regard to this latter observation, and in view of the incomplete nature of the historical record, it cannot be ruled out that the rate of seismic moment release and hence crustal shortening over periods of time greater than our 25-year sample are higher than what we have calculated; possibly comparable to the rates of relative plate motion predicted by plate tectonic models. The conclusion we are left with then is that, during the past 25 years, about 2.6–5.4 cm yr^{-1} of relative plate motion along the Taiwan plate boundary has been manifested by the occurrence of large earthquakes distributed within a broad region of the crust both onshore and off the east coast of Taiwan.

CONCLUSIONS

Large earthquakes that have occurred during the past 25 years near Taiwan show source depths that range from 13 to 88 km. Intermediate-depth events consistently show thrust-type mechanisms with T axes subparallel to the Wadati-Benioff zone, which is associated with the Ryukyu arc and likely reflect gravitational forces acting on the subducting slab. Shallow earthquakes (<30 km) are distributed over a broad zone along and off the east coast of Taiwan and show both high-angle reverse and strike-slip mechanisms. Deformation resulting from shallow earthquakes offshore northernmost Taiwan is interpreted to reflect not solely relative motion between the Philippine Sea and Eurasian plates, but also, relative motion between the Okinawa platelet and Taiwan, or complex deformation at the southwestern limit of the Ryukyu Trench. The shallow thrust and reverse-type earthquakes located both onshore and off the east coast of central and southern Taiwan show P axes that consistently trend in a northwest direction and are interpreted to reflect relative plate convergence between the Philippine Sea and the Eurasian plates. Hence relative plate motion, at least during the last 25 years, has not been taken up by slip along a simple thrust-type plate interface, as is characteristic of most convergent plate boundaries along the circum-Pacific, but by slip on faults distributed over a broad zone which extends along and off the east coast of Taiwan. Summation of the seismic moment tensors of the eight largest shallow earthquakes to have occurred since 1963 along and off the central and southern coast of Taiwan indicate that relative plate motion between the Eurasian and Philippine Sea plates has been accommodated by contraction of the crust at a rate of about 2.6–5.4 cm yr^{-1} during the last 25 years along an azimuth of about 290°.

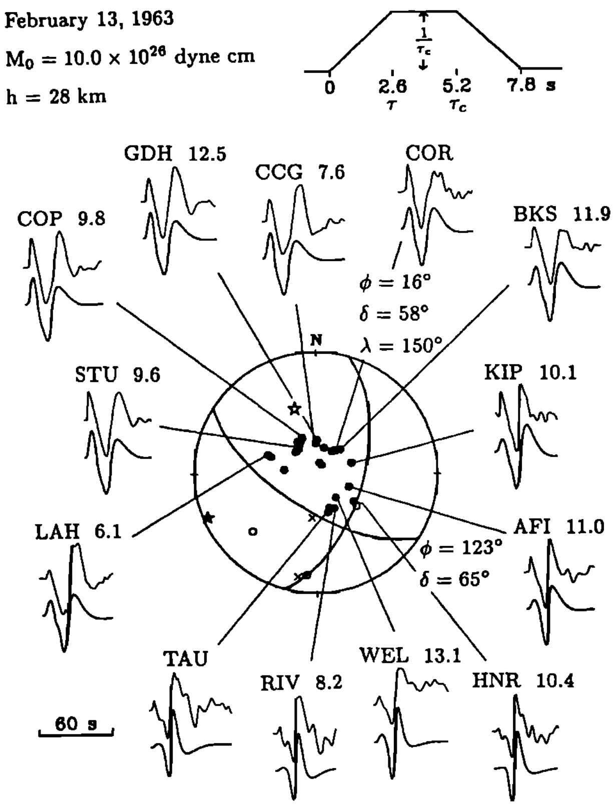

Fig. A1. E63. The mechanism determined here is similar to the mechanism ($\phi = 27°$, $\delta = 51°$, $\lambda = 159°$) determined by *Sudo* [1972*b*] using P wave first motions and the surface wave radiation pattern and significantly differs from the pure thrust mechanism ($\phi = 79°$, $\delta = 61°$, $\lambda = 90°$) determined from P wave first motions by *Katsumata and Sykes* [1969]. See text of appendix for explanation of symbols in this and all remaining figures of the appendix.

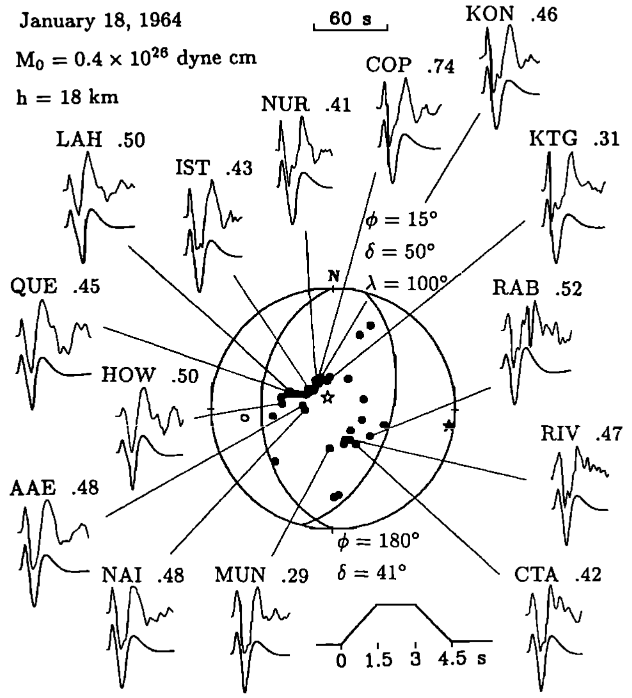

Fig. A2. Event E64. A slightly modified velocity and density structure is used to model this event because, unlike other events in this study, it is located beneath the island of Taiwan and not offshore. Source region P and S velocities and density ρ are assumed to be 7.0 km s^{-1}, 4.0 km s^{-1}, and 2.9 g cm^{-1}, respectively. Surface velocities are assumed to be 5.4 km s^{-1} for P waves and 3.1 km s^{-1} for S waves, and density ρ at the surface is 2.5 g cm^{-1}.

APPENDIX

Figures A1–A14 show the observed P wave first motions, comparisons of the synthetic to observed P and SH waveforms, and the focal mechanisms and source parameters for each of the earthquakes listed in Table 2 and shown in Figure 4. The figures are arranged in chronological order, and figure captions are limited to describing any unique aspects of the

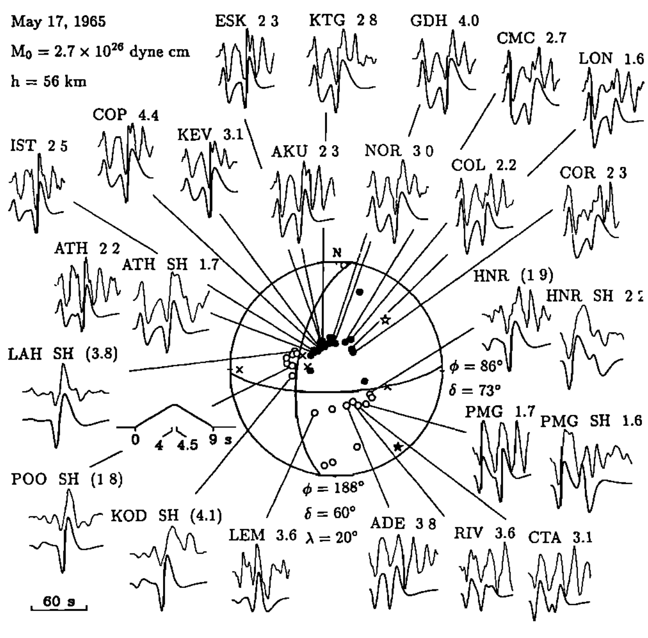

Fig. A3. Event E65.

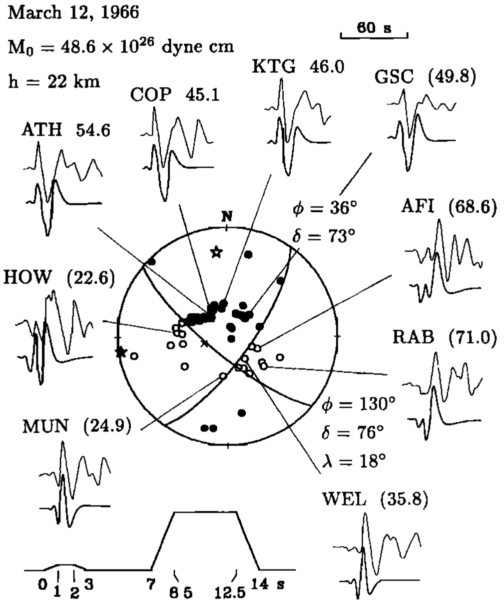

Fig. A4. Event E66M. The source time function is characterized by a small subevent that precedes the main event by about 4 s (Figure 9). The source time function of the small subevent (τ_c = 2.0 s) has one-tenth the amplitude of the source time function of the subsequent main event (τ_c = 5.5 s) and accounts for only 4% of the total M_0 = 48.6 × 10^{26} dyn cm. First motions of the initial foreshock at stations such as AFI, RAB, and WEL do not match well with the first motions predicted by the synthetic waveforms. Since we have assumed the same focal mechanism and location for both the subevent and main event, it appears that the initial subevent does not share the same focal mechanism as that of the main event. The mechanism determined here differs little from those published by *Sudo* [1972*b*] (ϕ = 125°, δ = 82°, λ = 45°) and *Wu* [1978] (ϕ = 114°, δ = 90°, λ = 36°).

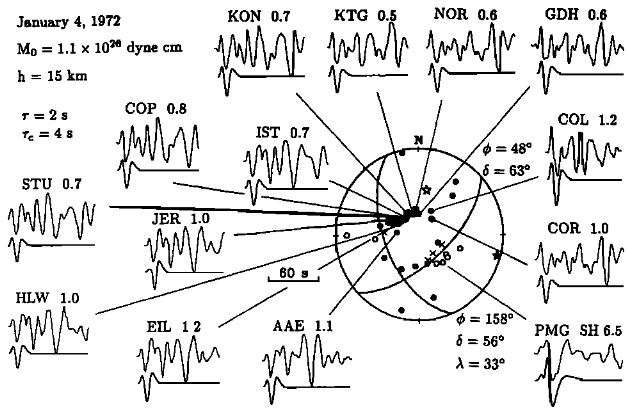

Fig. A6. Event E72J4. The observed P waveforms for this event are complex, with relatively large-amplitude energy arriving up to a minute or more after the first motion. In contrast, the single SH waveform observed at PMG (Δ = 40°) appears relatively simple. *Weins* [1987] interpreted similar observations to suggest that the P wave energy in such instances is likely due to prominent P wave reverberations in an overlying water layer. In general, the initial 15–20 s of the P waveforms are unaffected by the later arriving energy resulting from bounces in the water layer [e.g., *Lay and Okal*, 1983]. Hence, to first order, the source parameters of such earthquakes can be estimated by modeling the first cycle of the observed long-period waveforms [e.g., *Weins*, 1987; *Lay and Okal*, 1983].

event or comparison of results to prior studies of the respective earthquake. In that regard the format of each figure is as follows: Observed and synthetic P and SH waveforms correspond, respectively, to the upper and lower seismogram trace in each pair of seismograms shown. Focal

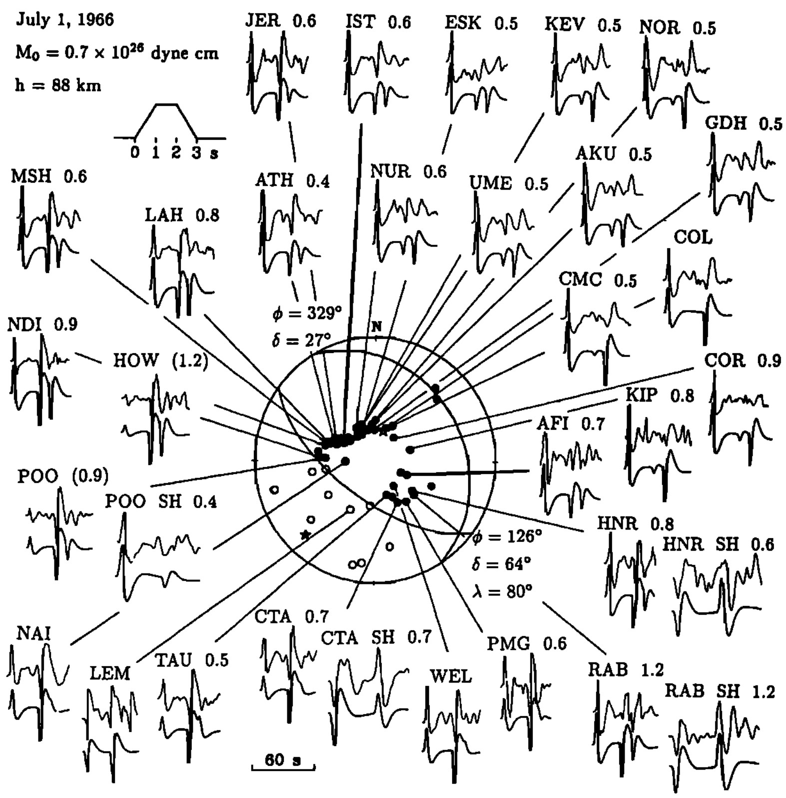

Fig. A5. Event E66J. The sS depth phase on SH waveforms at stations such as CTA and RAB unambiguously places the depth at about 88 km, although the sP phase in P waveforms recorded at stations to the north and northeast of the epicenter is conspicuously absent, as predicted by the synthetic waveforms.

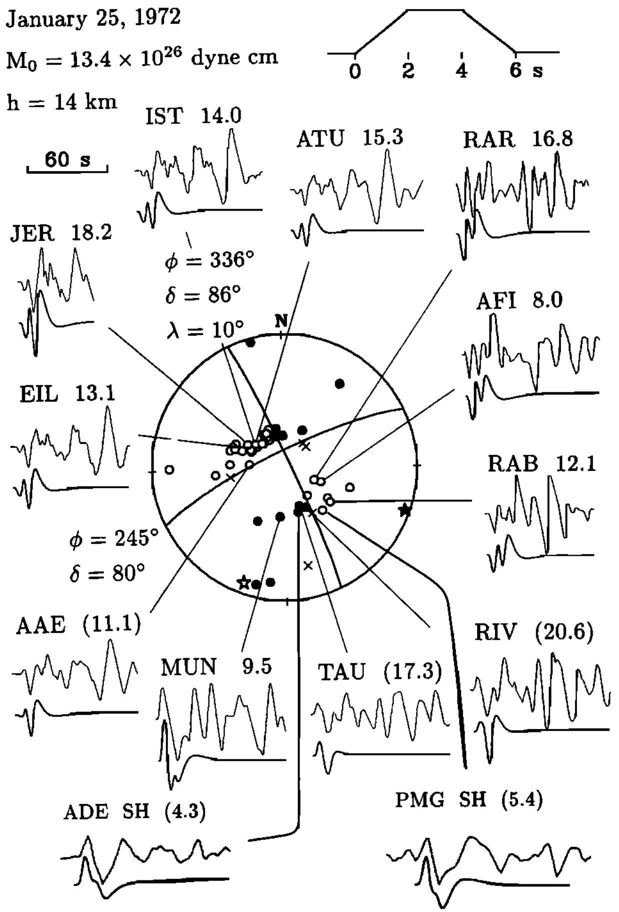

Fig. A7. Event E72J25. The *P* waveforms are complex and reverberate for more than a minute after the *P* wave first motion. Like event E72J4 (Figure A6), the relatively simple *SH* waveforms recovered at stations ADE and PMG are consistent with the interpretation that the long duration of *P* waveforms is also a result of water multiple reverberations. *Wu* [1978] studied aftershock patterns recorded by the local Taiwan network to infer that E72J25 occurred on the left-lateral and northwest striking nodal plane.

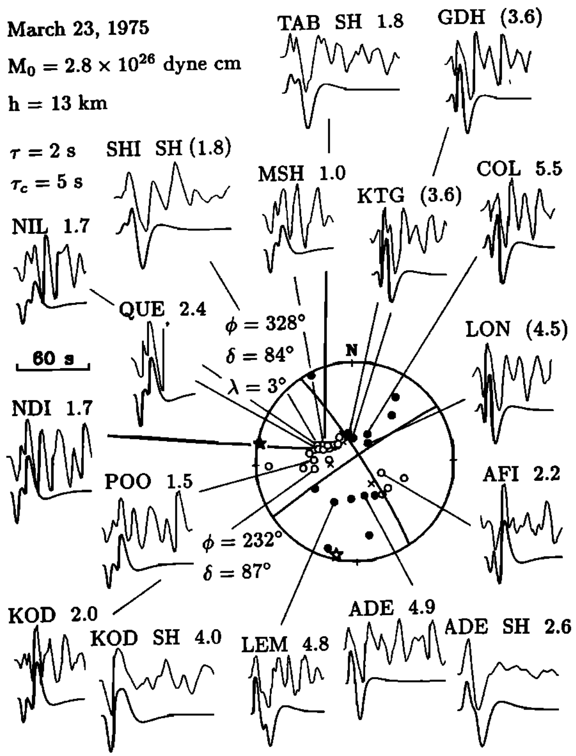

Fig. A8. Event E75. Like events E72J4 and E72J25, many of the *P* waveforms are characterized by large-amplitude cycles for up to a minute or more after the first arrival, but the available *SH* waveforms are relatively simple in character. Hence the energy arriving subsequent to the first 15–20 s of the *P* wave appears to result from the reverberations of the *P* wave in the overlying water layer [*Weins*, 1987]. *Wu* [1978] inferred left-lateral displacement along the northwest striking nodal plane based on aftershock patterns recorded by the local Taiwan network, although the four aftershocks reported by PDE (Figure 5) extend about 40 km along a northeast trend, suggesting rupture on the northeast striking nodal plane.

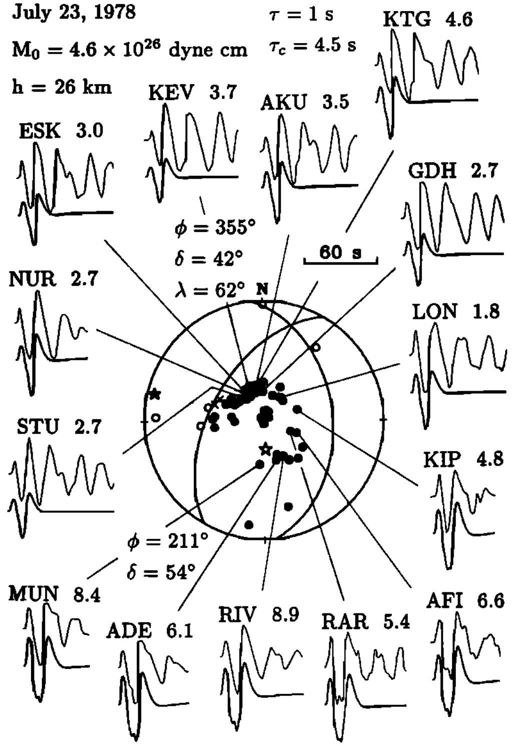

Fig. A9. Event E78J.

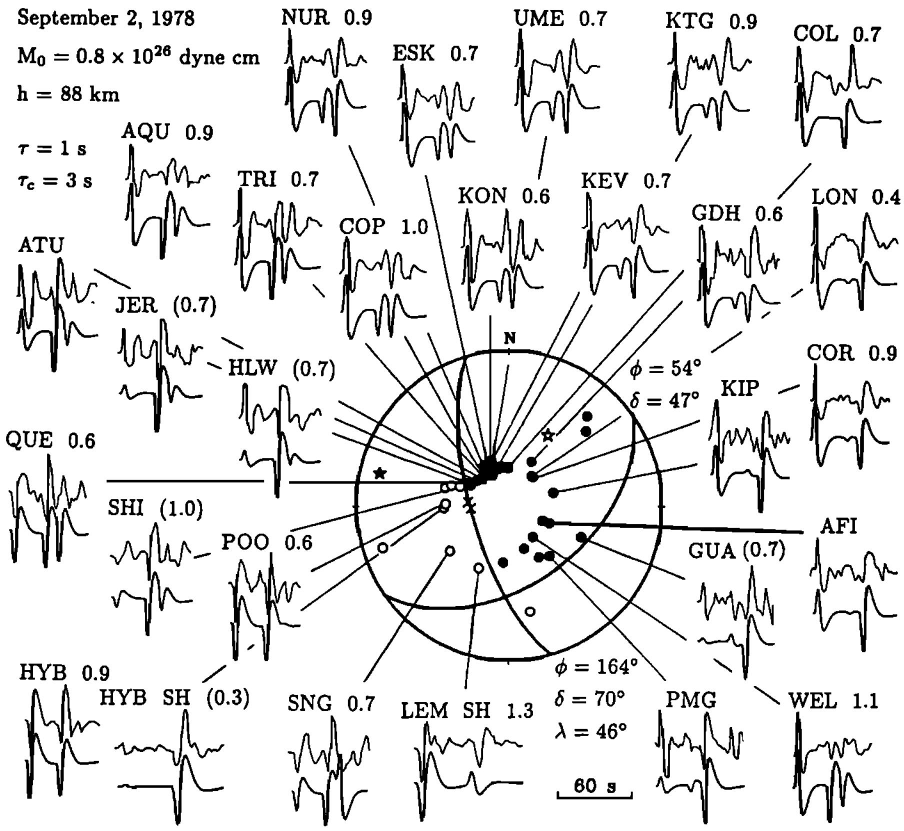

Fig. A10. Event E78S.

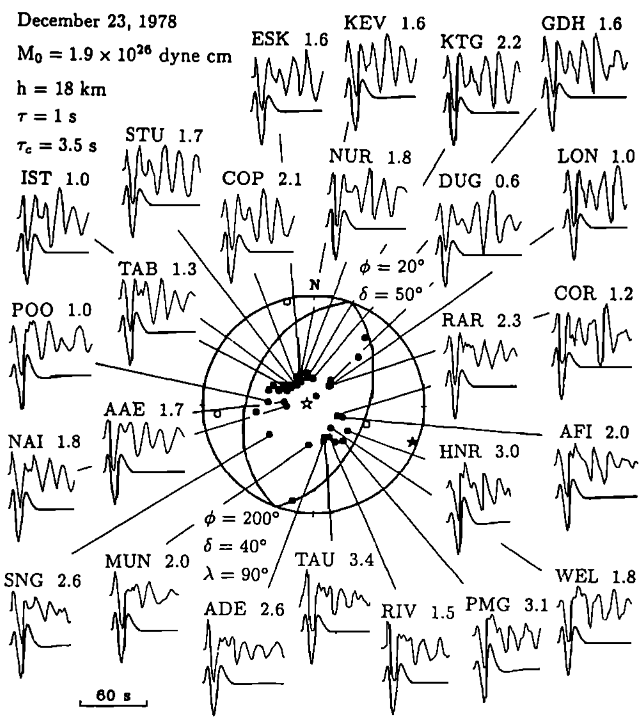

Fig. A11. Event E78D. Neither the waveform modeling nor the first motions provide firm limits on the orientation of the west dipping nodal plane.

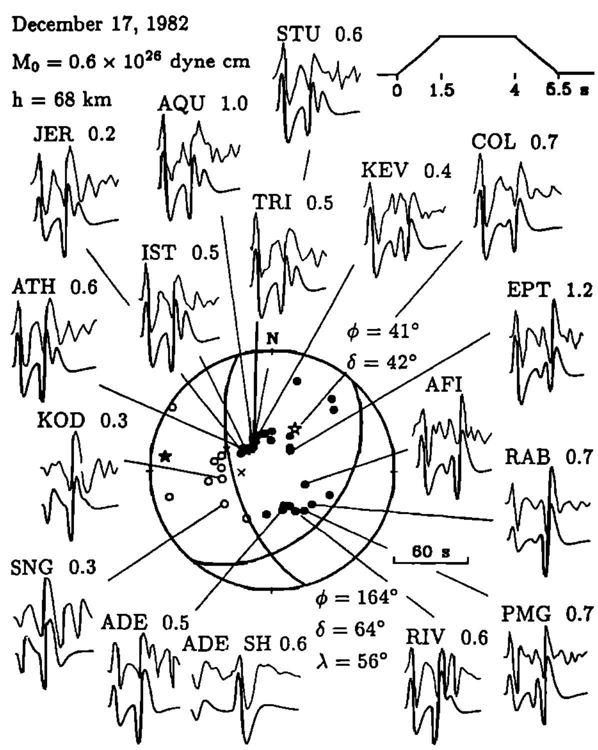

Fig. A12. Event E82: First motion data indicate a thrust mechanism for E82 but do little to limit the orientation of the east dipping nodal plane. Introducing a strike-slip component to the mechanism significantly improved the fit of the synthetics to the observed *SH* waveform at ADE and to the *P* wave depth phases.

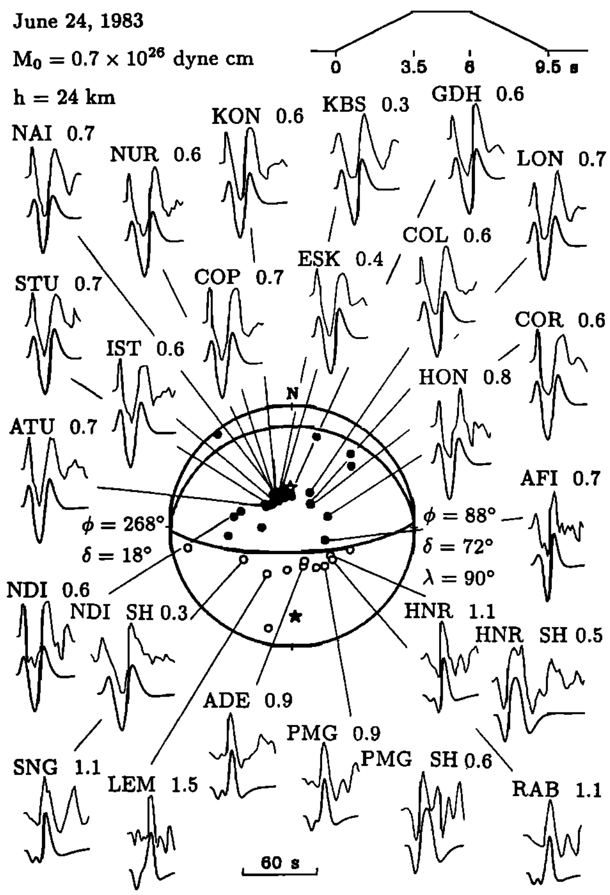

Fig. A13. Event E83.

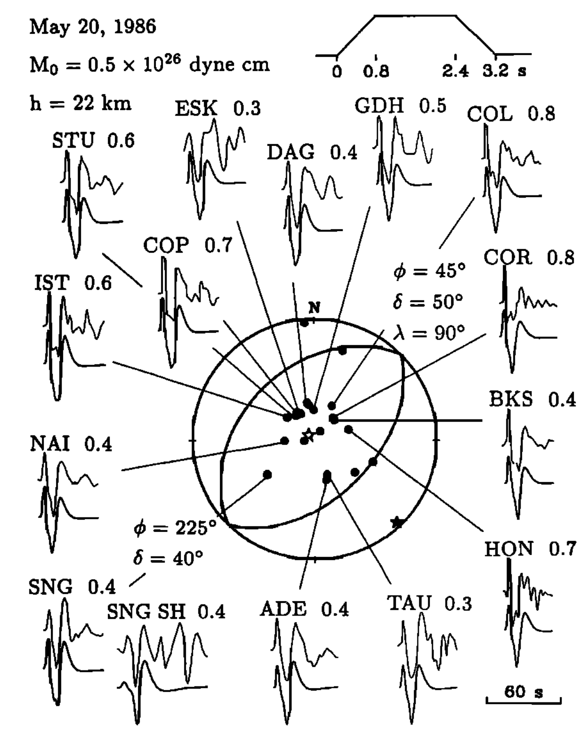

Fig. A14. Event E86M. The mechanism used to produce the synthetic seismograms and shown here is similar to the mechanism (ϕ = 35°, δ = 60°, λ = 90°) determined by *Chen and Wang* [1986] using data recorded on the Taiwan Telemetered Seismographic Network. *Chen and Wang* [1986] conclude that E86M was reverse faulting on the Longitudinal Valley fault, based on aftershock patterns that define rupture along a fault plane striking northeast and dipping southeast.

mechanisms are lower hemisphere and equal-area projections with compressional, dilatational, and nodal first motions indicated by solid circles, open circles, and x's, respectively. Solid and open stars indicate the location of the *P* and *T* axes, respectively. The synthetic seismograms correspond to the focal mechanism, source depth *h*, and source time function shown. Strike, dip, and rake of the nodal planes are ϕ, δ, and λ, respectively. Source time functions are assumed to be trapezoidal in shape and of unit area, characterized by a rise time τ and rupture duration τ_c. The seismic moment M_0 determined from individual waveforms is given beside each station in units of 10^{26} dyn cm. Estimates of seismic moment obtained at nodal stations are enclosed in parentheses. The value of seismic moment listed in the header of each figure is the value obtained by averaging the specific values of seismic moment obtained at nonnodal stations. *SH* waveforms are annotated with an SH and appear beside *P* waveforms at corresponding stations.

The body waves for event E86N, which occurred on November 14, 1986, were previously studied for separate purposes and in detail by *Hwang and Kanamori* [1989]. Hence we have used the results of their analysis in our study (Table 2) and do not show the waveforms for the event.

Acknowledgments. The manuscript has benefited from the reviews of Jacques Angelier, Wai-Ying Chung, Lisa R. Kanter, Steven W. Roecker, and Ross S. Stein. Lorraine J. Hwang kindly provided a preprint of a manuscript regarding the November 14, 1986, earthquake. Steven W. Roecker, Douglas A. Weins, and Francis T. Wu provided preprints, maps, and useful discussion. During the course of this study one of us (S.K.P.) was supported by a fellowship from the Center for Earthquake Research and Information. Research was supported in part by National Science Foundation grant EAR-86-18314.

REFERENCES

Abe, K., Magnitudes of large shallow earthquakes from 1904 to 1980, *Phys. Earth Planet. Inter.*, *27*, 72–92, 1981.

Allen, C. R., Circum-Pacific faulting in the Philippine-Taiwan region, *J. Geophys. Res.*, *67*, 4795–4812, 1962.

Angelier, J., Preface: Geodynamics of the Eurasia-Philippine Sea plate boundary, *Tectonophysics*, *125*, IX–X, 1986.

Aki, K., and P. G. Richards, *Quantitative Seismology: Theory and Methods*, W. Freeman Cooper, San Francisco, Calif., 1980.

Astiz, L., Study of intermediate-depth earthquakes and interplate coupling, Ph.D. dissertation, Calif. Inst. of Technol., Pasadena Calif., 1987.

Barrier, E., The two stage collision of Taiwan: An active orogen, *Tectonophysics*, *115*, 167–175, 1985.

Barrier, E., and J. Angelier, Active collision in eastern Taiwan: The Coastal Range, *Tectonophysics*, *125*, 39–72, 1986.

Biq, C. C., Some aspects of post-orogenic block tectonics in Taiwan, Recent crustal movements, *Bull. R. Soc. N. Z.*, *9*, 19–24, 1971.

Bonilla, M. G., A review of recently active faults in Taiwan, *U.S. Geol. Surv. Open File Rep.*, *75-41*, 58, 1975.

Bowin, C., S. R. Lu, C. H. Lee, and H. Schouten, Plate convergence and accretion in Taiwan-Luzon region, *Am. Assoc. Pet. Geol. Bull.*, *62*, 1645–1672, 1978.

Brune, J. N., Seismic moment, seismicity, and rate of slip along major fault zones, *J. Geophys. Res.*, *67*, 4795–4812, 1968.

Chai, B. H. T., Structure and tectonic evolution of Taiwan, *Am. J. Sci.*, *272*, 389–422, 1972.

Chase, C. G., Plate kinematics: The Americas, east Africa and the rest of the world, *Earth Planet. Sci. Lett.*, *37*, 355–368, 1978.

Chen, K. C., and J. H. Wang, The May 20, 1986 Hualien, Taiwan earthquake and its aftershocks, *Acad. Sin. Bull. Inst. Earth Sci.*, *6*, 1–13, 1986.

Davis, D., J. Suppe, and F. A. Dahlen, Mechanics of fold-and-thrust belts and accretionary wedges, *J. Geophys. Res.*, *88*, 1153–1172, 1983.

Fitch, T. J., Plate convergence, transcurrent faults, and internal deformation adjacent to Southeast Asia and the Western Pacific, *J. Geophys. Res.*, *77*, 4432–4460, 1972.

Futterman, W. I., Dispersive body waves, *J. Geophys. Res.*, *67*, 5279–5291, 1962.

Gutenberg, B., and C. F. Richter, Seismicity of the Earth and Associated Phenomena, 2nd ed., 310 pp., Princeton University Press, Princeton, N. J., 1954.

Hagen, R. A., F. K. Duennebier, and V. Hsu, A seismic refraction study of the crustal structure in the active seismic zone east of Taiwan, *J. Geophys. Res.*, *93*, 4785–4796, 1988.

Ho, C. S., A synthesis of the geologic evolution of Taiwan, *Tectonophysics*, *125*, 1–16, 1986.

Hsu, T. L., Recent faulting in the Longitudinal Valley of Eastern Taiwan, *Mem. Geol. Soc. China*, *1*, 95–102, 1962.

Hsu, T. L., Seismicity of Taiwan and some related problems, *Bull. Int. Seismol. Earthquake Eng.*, *8*, 41–61, 1971.

Huchon, P., E. Barrier, J. C. De Bremaecker, and J. Angelier, Collision and stress trajectories in Taiwan: A finite element model, *Tectonophysics*, *125*, 179–191, 1986.

Hwang, L. J., and H. Kanamori, Teleseismic and strong motion source spectra from two earthquakes in eastern Taiwan, *Bull. Seismol. Soc. Am.*, in press, 1989.

Isacks, B., and P. Molnar, Mantle earthquake mechanisms and the sinking of the lithosphere, *Nature*, *223*, 1121–1124, 1969.

Jahn, B., Reinterpretation of geologic evolution of the coastal range, eastern Taiwan, *Geol. Soc. Am. Bull.*, *83*, 241, 1972.

Jahn, B. M., F. Martineau, J. J. Peucat, and J. Cornichet, Geochronology of the Tananao schist complex, Taiwan, and its regional tectonic significance, *Tectonophysics*, *125*, 103–124, 1986.

Juan, V. C., Tectonic evolution of Taiwan, *Tectonophysics*, *26*, 197–212, 1975.

Juan, V. C., H. J. Lo, and C. H. Chen, Geotectonics of Taiwan—An overview in *Geodynamics of the Western Pacific, Advances in Earth and Planetary Sciences*, vol. 6, edited by S. Uyeda, R. W. Murphy, and K. Kobayashi, pp. 379–386, Center for Academic Publication, Tokyo, Japan, 1980.

Kanamori, H., Magnitude scale and quantification of earthquakes, *Tectonophysics*, *93*, 185–199, 1983.

Karig, D. E., Plate convergence between the Philippines and the Ryukyu Islands, *Mar. Geol.*, *14*, 153–168, 1973.

Katsumata, M., and L. R. Sykes, Seismicity and tectonics of the Western Pacific: Izu-Mariana-Caroline and Ryukyu-Taiwan regions, *J. Geophys. Res.*, *74*, 5923–5948, 1969.

Kostrov, B. V., Seismic moment and energy of earthquakes, and seismic flow of rock, *Izv. Acad. Sci. USSR Phys. Solid Earth, Engl. Transl.*, *1*, 23–40, 1974.

Langston, C. A., and D. V. Helmberger, A procedure for modelling shallow dislocation sources, *Geophys. J. R. Astron. Soc.*, *42*, 117–130, 1975.

Lay, T., and E. Okal, The Gilbert Islands (Republic of Kiribati) earthquake swarm of 1981-1983, *Phys. Earth Planet. Inter.*, *21*, 283–304, 1983.

Lee, T. Q., J. S. Liaw, and Y. B. Tsai, Further evidence for subduction of the Philippine Sea Plate underneath northern Taiwan, *Proc. Geol. Soc. China*, *21*, 168–175, 1978.

Minster, J. B., and T. H. Jordan, Rotation vectors for the Philippine and Rivera plates (abstract), *Eos Trans. AGU*, *60*, 958, 1979.

Morgan, W. J., Plate motions and deep mantle convection, *Mem. Geol. Soc. Am.*, *132*, 7–21, 1972.

Pelletier, B., and J. F. Stephan, Middle Miocene obduction and Late Miocene beginning of collision registered in the Hengchun Peninsula: Geodynamic implications for the evolution of Taiwan, *Tectonophysics*, *125*, 133–160, 1986.

Roecker, S. W., Y. H. Yeh, and Y. B. Tsai, Three-dimensional *P* and *S* wave velocity structures beneath Taiwan: Deep structures beneath an arc-continent collision, *J. Geophys. Res.*, *92*, 10,547–10,570, 1987.

Rowlett, H., and J. Kelleher, Evolving seismic and tectonic patterns along the western margin of the Philippine Sea plate, *J. Geophys. Res.*, *81*, 3518–3524, 1976.

Ruff, L., and H. Kanamori, Seismic coupling and uncoupling at subduction zones, *Tectonophysics*, *99*, 99–117, 1983.

Seno, T., The instantaneous rotation vector of the Philippine Sea plate relative to the Eurasian plate, *Tectonophysics*, *42*, 209–226, 1977.

Seno, T., and T. Eguchi, Seismotectonics of the Western Pacific region, in *Geodynamics of the Western Pacific-Indonesian Region, Geodyn. Ser.*, vol. 11, edited by T. W. C. Hilde and S. Uyeda, pp. 5–40, AGU, Washington, D. C., 1983.

Seno, T., and K. Kurita, Focal mechanisms and tectonics in the Taiwan Philippine region, in *Geodynamics of the Western Pacific, Advances in Earth and Planetary Sciences*, vol. 6, edited by S. Uyeda, R. W. Murphy, and K. Kobayashi, pp. 249–263, Center for Academic Publication, Tokyo, Japan, 1979.

Seno, T., T. Moriyama, S. Stein, D. F. Woods, C. Demets, D. Argus, R. Gordon, Redetermination of the Philippine Sea Plate motion (abstract), *Eos Trans. AGU*, *68*, 1474, 1987.

Sibuet, J-C, J. Letouzey, F. Barbier, J. Charvet, J.-P. Foucher, T. W. C. Hilde, M. Kimura, C. Ling-Yun, B. Marsset, C. Muller, and J. F. Stephan, Back arc extension in the Okinawa Trough, *J. Geophys. Res.*, *92*, 14,041–14,063, 1987.

Sudo, K., Two distinct phases in the initial *P*-wave group of the Niigata earthquake of 1964 and of the Taiwan-oki earthquake of 1966, *J. Phys. Earth*, *20*, 111–125, 1972*a*.

Sudo, K., The focal process of the Taiwan-Oki earthquake of March 12, 1966, *J. Phys. Earth*, *20*, 147–164, 1972*b*.

Suppe, J., The active Taiwan mountain belt, in *The Anatomy of Mountain Ranges*, edited by J.-P. Schaer, and J. Rodgers, pp. 277–293, Princeton University Press, Princeton, N. J., 1987.

Taira, K., Holocene crustal movements in Taiwan as indicated by radiocarbon dating of marine fossils and driftwood, *Tectonophysics*, *28*, T1–T5, 1975.

Tsai, Y. B., A study of disastrous earthquakes in Taiwan, 1683-1895, *Acad. Sin. Bull. Inst. Earth Sci.*, *5*, 1–44, 1985.

Tsai, Y. B., Seismotectonics of Taiwan, *Tectonophysics*, *125*, 17–37, 1986.

Weins, D. A., Effects of near source bathymetry on teleseismic *P*-waveforms, *Geophys. Res. Lett*, *14*, 761–764, 1987.

Wu, F. T., Focal mechanisms and tectonics in the vicinity of Taiwan, *Bull. Seismol. Soc. Am.*, *60*, 2045–2056, 1970.

Wu, F. T., Recent tectonics of Taiwan, *J. Phys. Earth*, *26*, S265–S299, 1978.

York, J. E., Quaternary faulting in Eastern Taiwan, *Bull. Geol. Surv. Taiwan*, *25*, 63–72, 1976.

S. K. Pezzopane, Department of Geology, University of Oregon, Eugene, OR 97403.

S. G. Wesnousky, Center for Earthquake Research and Information, Memphis State University, Memphis, TN 38152.

(Received July 29, 1988;
revised February 9, 1989;
accepted February 15, 1989.)